On the mechanism of polarized metre-wave stellar emission

Vedantham, H. K.

Published in:
Monthly Notices of the Royal Astronomical Society

DOI:
10.1093/mnras/staa3373

Publication date:
2021

Monthly Notices of the ROYAL ASTRONOMICAL SOCIETY

MNRAS **500,** 3898–3907 (2021) doi:10.1093/mnras/staa3373
Advance Access publication 2020 November 2

On the mechanism of polarized metre-wave stellar emission

H. K. Vedantham [1,2]★

[1]*ASTRON, The Netherlands Institute for Radio Astronomy, Oude Hogeveensedijk 4, NL-7991PD Dwingeloo, the Netherlands*
[2]*Kapteyn Astronomical Institute, University of Groningen, Landleven 12, NL-9747AD Groningen, the Netherlands*

Accepted 2020 October 12. Received 2020 October 11; in original form 2020 April 30

ABSTRACT

Two coherent radio emission mechanisms operate in stellar coronae: plasma emission and cyclotron emission. They directly probe the electron density and magnetic field strength respectively. Most stellar radio detections have been made at cm-wavelengths where it is often not possible to uniquely identify the emission mechanism, hindering the utility of radio observations in probing coronal conditions. In anticipation of stellar observations from a suite of sensitive low-frequency ($\nu \sim 10^2$ MHz) radio telescopes, here I apply the general theory of coherent emission in non-relativistic plasma to the low-frequency case. I consider the recently reported low-frequency emission from dMe flare stars AD Leo and UV Ceti and the quiescent star GJ 1151 as test cases. My main conclusion is that unlike the cm-wave regime, for reasonable turbulence saturation regimes, the emission mechanism in metre-wave observations ($\nu \sim 10^2$ MHz) can often be identified based on the observed brightness temperature, emission duration, and polarization fraction. I arrive at the following heuristic: M-dwarf emission that is $\gtrsim$ hour-long with $\gtrsim$50 per cent circular polarized fraction at brightness temperatures of $\gtrsim 10^{12}$ K at $\sim$100 MHz in M-dwarfs strongly favours a cyclotron maser interpretation.

Key words: radiation mechanisms: non-thermal – stars: coronae – radio continuum: stars.

1 INTRODUCTION

Several low-frequency ($\nu \sim 10^2$ MHz) observational efforts aim to study stellar coronal activity and exoplanetary magnetospheres (Bastian, Dulk & Leblanc 2000; Murphy et al. 2015; Lynch et al. 2017a, b; O'Gorman et al. 2018; Turner et al. 2019; Villadsen & Hallinan 2019; Vedantham et al. 2020). At metre-wavelengths, existing telescopes are only sensitive to radiation with very high brightness temperatures ($\gg 10^{10}$ K) that favour a coherent emission process. Observations of coherent emission are particularly constraining since they provide a clean measurement of the plasma density (in case of plasma emission) and magnetic field strength (in case of cyclotron emission) in the emitter.

Highly polarized radio bursts have been studied at cm-wavelength. The implied plasma densities and magnetic field strengths for the case of plasma and cyclotron emission are $\sim 10^{11}$ cm^{-3} and $\sim 10^3$ G, respectively. The emission site is likely to reside in coronal magnetic loops with heights significantly smaller than the stellar radius. A secure determination of the field strength and plasma density is however only possible if the emission mechanism can be uniquely identified. This is in general not straightforward; both emission mechanisms have been suggested to account for observations with comparable characteristics (Melrose & Dulk 1982; Zaĭtsev & Stepanov 1983; Stepanov et al. 2001; Slee, Willes & Robinson 2003; Villadsen & Hallinan 2019; Zic et al. 2019)

Metre-wavelengths are sensitive to much lower densities ($\sim 10^8$–10^9 cm^{-3}) and field strengths ($B \sim 10^2$ G) that are likely to persist at coronal heights comparable to or larger than the stellar radius. They, therefore, probe the tenuous higher coronal layers where one anticipates a transition between a radial coronal structure dictated by hydrostatic balance to one determined by the outflowing stellar wind, and occasionally, coronal mass ejections. Such data are of acute interest because they can be used to infer the space weather conditions around exoplanets.

Large metre-wavelength radio telescopes capable of mJy-level sensitivities are now available (Tingay et al. 2013; van Haarlem et al. 2013; Gupta et al. 2017). Coherent emission can attain brightness temperature of $\gtrsim 10^{12}$ K which yields a distance-horizon of $\gtrsim$10 pc for mJy-level sensitivity – sufficient for an unbiased survey of stars of varying spectral-type and activity levels. In anticipation of a sumptuous yield of metre-wave stellar bursts (and perhaps exoplanetary emissions) from these surveys, I review the basic theory of coherent emissions and propagation, with a particular emphasis on metre-wavelengths (Section 2).

Targeted observations of anomalously active flare stars have recently detected several coherent radio bursts at metre-wavelengths. While such stars are not representative of the vast majority of quiescent stars, the observations provide a fortuitous opportunity to apply the basic principles of coherent emission in coronae. I undertake this in Section 3.

The main conclusion I reach is that for $\nu \sim 10^2$ MHz, a brightness temperature that exceeds $\sim 10^{12}$ K and high polarization fraction ($\gtrsim$50 per cent) favours a cyclotron maser interpretation for prototypical of M-dwarf coronal parameters. In some highly active stars, the increases coronal temperature and density scale height might lead to highly polarized plasma emission reaching a brightness temperature of $\sim 10^{12}$ K. On the other hand, in the cm-wave regime, the intensity of observed long-duration emission can be explained by both cyclotron maser and plasma emission. Hence low-frequency observations of stellar bursts will usually lead to a clear identification of the emission mechanism.

★ E-mail: vedantham@astron.nl

A glossary of symbols and their meaning is given in the Appendix for quick reference. I use Gaussian units unless specified otherwise.

2 COHERENT EMISSION MECHANISMS

There are two known coherent emission mechanisms in non-relativistic plasma: cyclotron emission and plasma emission. While reviewing the necessary theory here, I only present the basic equations and first-principles here, and refer the reader to the original sources: Benz (1993), Melrose & Dulk (1982), Zaĭtsev & Stepanov (1983), Wu & Lee (1979), and Treumann (2006) for further details.

2.1 Cyclotron maser

Cyclotron maser emission occurs at the fundamental and harmonics of the cyclotron frequency: $\nu_c \approx 2.8 \times 10^6\, B$, where B is the ambient magnetic field strength. The source of free energy in cyclotron maser is an inverted (or unstable) population of electrons. In the two-dimensional momentum space (axis parallel and perpendicular to the magnetic field), the inversion usually takes the form of either a loss-cone or horseshoe-shaped distribution[1] of *mildly relativistic* electrons ($E \gtrsim 10$ keV). The horseshoe-type maser can generate brightness temperatures that are orders of magnitude larger than that from a loss-cone distribution, but in general, requires an accelerating electric field that is parallel to the magnetic field. It is presently unclear if such an electric field can be sustained over long periods in a dense corona which can readily shield such fields. The loss-cone, on the other hand, can be readily established via magnetic mirroring in a magnetic trap such as a coronal loop or the large-scale magnetic field of an object. Consequently, horseshoe masers are generally thought to drive auroral emissions in the rarefied magnetospheres of the planets, and possibly some short-duration ($\ll$1 s) 'spike-bursts' in stellar coronae. Because, we are only considering long-duration emission here, we assume that any cyclotron maser emission from corona must be of the loss-cone type.

The theory of loss-cone masers has been studied extensively. Here we adopt expressions from Melrose & Dulk (1982) for the radiation brightness temperature. Let the maser be driven by a non-thermal population of mildly relativistic electrons with a density n_o and characteristic speed v_0. The maximum attainable brightness temperature in a loss-cone maser is

$$T_b^{max} \approx \frac{1}{2\pi}\left(\frac{n_o m_e v_o^2}{k_B}\right)\left(\frac{c^2}{\nu v_o}\right)^3. \quad (1)$$

The first term within parentheses is the kinetic energy density in the emitting electrons which for $v_o = 0.2c$ is $\sim n_o 10^8$ K. The peak brightness temperature is therefore

$$T_b^{max} \approx 5 \times 10^{16} n_0 \beta_{0.2}^{-1} \nu_{100}^{-3}. \quad (2)$$

The finite rate at which the loss cone forms and empties reduces the brightness temperature of the time-averaged emission by a factor of $v_o/(\Gamma L)$ where Γ is the growth rate of the maser, L is the length-scale of the magnetic trap (v_o/L is the rate at which the loss-cone forms). The resulting time-averaged brightness temperature is

$$T_b^{avg} \approx \frac{m_e v_0^2}{4\pi k_B}\frac{c^2}{\nu^2 L r_0}, \quad (3)$$

where r_0 is the classical electron radius. In convenient units, we have

$$T_B^{avg} \approx 10^{14.8}\, \beta_{0.2}^2 \nu_{100}^{-2}\left(\frac{L}{10^{10}\,\mathrm{cm}}\right)^{-1}. \quad (4)$$

Individual spikes can attain brightness approaching T_b^{max}, but only with a small duty factor. The time-averaged brightness temperature cannot exceed T_b^{avg}.

The polarization of cyclotron maser emission is ≈100 per cent in the *x*- or *o*-mode depending on whether emission at the fundamental or the second harmonic has the higher growth rate allowing it to extract most of the available free energy.[2] In a loss-cone driven maser, for $\nu_p/\nu_c \lesssim 0.2$, x-mode at the fundamental cyclotron frequency is expected to dominate, whereas o-mode at the fundamental or the x-mode at the second harmonic will dominate at higher ratios.

Cyclotron maser adequately describes the emission properties of all magnetized Solar system planets. Although such emission must occur in stellar coronae, cyclotron absorption by dense ambient thermal plasma in stellar coronae requires one to postulate an additional mechanism to ensure radiation escape. Because cyclotron absorption falls rapidly for small angles between the magnetic field and the wave vector (details in Appendix A), the proposed mechanisms invariable involve guiding the emitted energy along magnetic field lines, via some scattering mechanism (see for e.g. Zaĭtsev, Shaposhnikov & Rucker 2005) or via wave refraction (see for e.g. Speirs et al. 2014).

To convert observed flux densities to brightness temperature, we need the transverse emitter size. This must be determined jointly by (a) the beaming properties and instantaneous bandwidth of the maser and (b) the 'active' section of the source to which the mildly relativistic electrons driving the maser are confined. The latter especially depends on the electron acceleration mechanism which is not known a priori. For simplicity, we assume that the emitter is a circle of radius xR_* where R_* is the physical radius of the emitting object. If F is the observed flux density, then the observationally inferred brightness temperature is

$$T_b^{obs} = \frac{F\lambda^2}{2k_B}\frac{d^2}{\pi x^2 R_*^2} \approx 10^{13}\frac{F}{\mathrm{mJy}}\nu_{100}^{-2}x^{-2}R_{*,10}^{-2}d_{10}^2\ \mathrm{K}. \quad (5)$$

Comparing this with the theoretical estimate, we find that loss-cone driven masers on stars at $d \sim 10$ pc can reach ∼mJy level flux densities at 100 MHz.

2.2 Plasma emission

As before, I present the final equations and basic arguments here and refer the reader to Appendix B and the original sources (Zaĭtsev & Stepanov 1983; Benz 1993; Stepanov et al. 1999; Stepanov et al. 2001) for further details. Plasma emission occurs at the fundamental or harmonic of the plasma frequency: $\nu_p \approx 10^4 n_e^{0.5}$. The energy source for coronal plasma emission is the turbulent injection of impulsively heated plasma into an ambient cooler and denser medium. Such a situation can likely persist in confined plasma in flaring coronal loops. Emission at the fundamental plasma frequency is generated by scattering of plasma density waves (called Langmuir waves) on thermal ions. Emission at the second harmonic is generated by coalescence of two Langmuir waves travelling in opposite directions.

[1]Loss cone refers to an absence of gyrating electrons at low pitch angles creating a population inversion in perpendicular (to the B-field) momentum space that drives the maser.

[2]The two nature modes in a magnetized plasma are elliptically polarized with axial ratios of T_x and $T_o = -1/T_x$. *x*-mode has an electric field rotating in the same sense as the gyrating electrons.

Detailed expressions for the relevant emission and absorption coefficient have been derived elsewhere. Here I use the expressions for emergent brightness temperature given by Stepanov et al. (2001) that include the effects of spontaneous emission along with the non-linear effects of absorption by collisional damping and induced emission. At very low frequencies and for typical density scale heights in M-dwarfs coronae, the brightness temperatures derived by assuming spontaneous emission in an optically thin source are good approximations (as will be evident later). I, therefore, present these approximate equations here (further details in the Appendix B) while cautioning the reader that they may not be applicable at cm-wavelengths.

The brightness temperature for optical thin fundamental and second harmonic plasma emission are given by

$$T_{\rm b,f} \sim 2\times10^{10}\nu_{100}\left(\frac{h_{\rm p}}{10^{10}\,{\rm cm}}\right)\left(\frac{T_{\rm l}}{10^{8}\,{\rm K}}\right)\left(\frac{w}{10^{-5}}\right) \quad (6)$$

and

$$T_{\rm b,h} \sim 4\times10^{10}\left(\frac{h_{\rm p}}{10^{10}\,{\rm cm}}\right)\left(\frac{T}{10^{6}\,{\rm K}}\right)^{4}\left(\frac{T_{\rm l}}{10^{8}\,{\rm K}}\right)^{-1/2}\left(\frac{w}{10^{-5}}\right)^{2}. \quad (7)$$

The brightness temperatures cannot be arbitrarily large and will saturate at some level. At metre-wavelengths, harmonic emission dominates and is most likely to saturate (Stepanov et al. 2001). This is especially true in flare stars with hot coronae because $T_{\rm b,h}\propto h_{\rm p}T^{4}\propto T^{5}$. Saturation happens when the brightness temperature of emission equals that of the Langmuir waves (Melrose 1980) given by

$$T_{\rm b,h}^{\rm max} \sim 10^{12}\left(\frac{\nu_{\rm p}}{100\,{\rm MHz}}\right)^{-1}\left(\frac{T}{10^{6}\,{\rm K}}\right)^{3/2}\left(\frac{T_{\rm l}}{5\times10^{7}\,{\rm K}}\right). \quad (8)$$

The beaming pattern of plasma emission at both the fundamental and harmonic is broad. Because a stellar disc may not be filled entirely by flaring loops, I take the transverse area of the emitter to be a fraction f of the stellar disc. The observed flux density then has a simple relationship to the brightness temperature of the emitter:

$$T_{\rm b}^{\rm obs} = \frac{F\lambda^{2}d^{2}}{2k_{\rm B}f\pi R_{*}^{2}} \approx 10^{14}\nu_{100}^{-2}d_{10}^{2}R_{*,10}^{-2}\left(\frac{f}{0.1}\right)^{-1}\left(\frac{F}{\rm mJy}\right)\,{\rm K}. \quad (9)$$

Even if $f\approx1$ (entire disc is filled with flaring loops), it is clear from equations (9) and (6) that fundamental plasma emission is unlikely to generate a ∼mJy level source at $d\sim10\,$pc at $\nu\sim100\,$MHz. However in much hotter coronae with $T\approx5\times10^{6}\,$K, a comparison of equations (9) and (7) shows that the second harmonic emission may generate a ∼mJy level source with the above assumptions.

2.2.1 *Polarization of plasma emission*

Fundamental plasma emission is ≈100 per cent polarized in the o-mode. Second harmonic plasma emission from solar bursts are only seen to have moderate polarization fractions of $\lesssim$20 per cent, but this is likely due to lower magnetic field strength in the solar corona. At higher magnetic field strengths which are likely to be encountered in coronae of late-type stars, the theory allows higher polarization fractions.

Second harmonic emission can be polarized in either x- or o-mode depending on whether the Langmuir wave spectrum is isotropic or preferentially beamed. The polarization fraction in the two cases is $\approx1.8|\cos\theta|\nu_{\rm c}/\nu_{\rm p}$ and $0.23|\cos\theta|\nu_{\rm c}/\nu_{\rm p}$ respectively, where θ is the angle between the wave vector and the magnetic field. These are approximations valid for $\nu_{\rm c}\ll\nu_{\rm p}$, which is likely true in the solar corona but not necessarily the case in other stars, especially M-dwarfs with strong magnetic fields. Melrose et al. (1980) have derived analytic expressions for the general case, which I have computed and plotted in Fig. 1 for the case of isotropic Langmuir wave spectrum (see Appendix C for details). The figure shows that angle averaged polarization fractions of up to ≈75 per cent in the x-mode are feasible for $\nu_{\rm p}/\nu_{\rm c}\approx0.6$. At lower ratios, the polarized fraction drops quasi-linearly and at higher ratios, gyro-harmonic absorption at the $s=3$ layer allows radiation escape only in contrived geometries (see Appendix A for details).

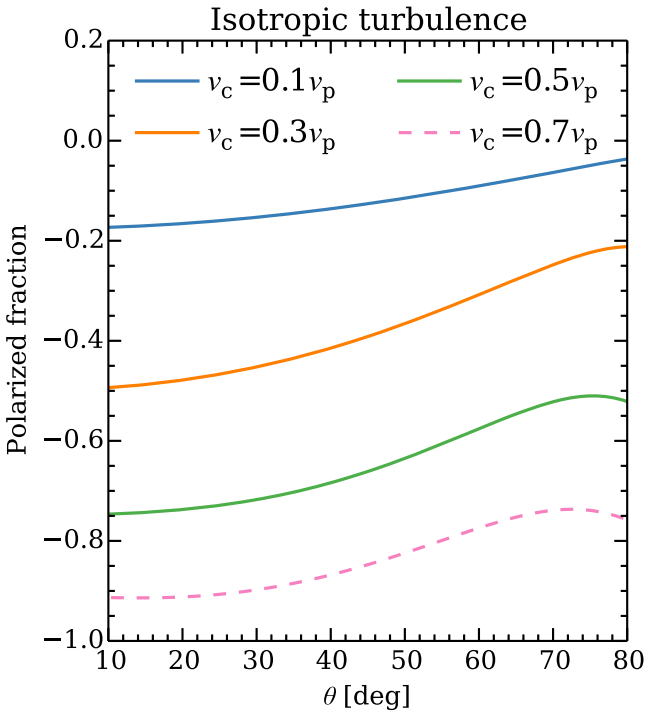

Figure 1. Polarization of second harmonic emission excited by an isotropic distribution of Langmuir waves as a function of the angle between wave vector and the magnetic field. The curves were computed using the analytic expression given by Melrose et al. (1980). The curves are for different values of plasma to cyclotron frequency ratio. Negative polarization indicates x-mode dominated emission. The dotted line implies that radiation escape is only possible in contrived geometries (for $\nu_{\rm c}/\nu_{\rm p}\gtrsim0.6$; see Appendices A and C for details).

The observed polarization of second harmonic radiation over a broad bandwidth will be lower because the ratio $\nu_{\rm p}/\nu_{\rm c}$ will invariably vary within coronal loops. Additionally, the observed polarized fraction of the fundamental and the harmonic will be lowered due to superposition of emission of opposite polarity from regions of positive and negative line-of-sight magnetic field components. If the size of the emitter is a large fraction of the surface area of the star, then in the absence of a special viewing geometry, the emission will be a nearby equal mix of waves with opposing polarities and the aggregate radiation will be unpolarized. As such, low polarization fractions are expected if the size of the emitter is a substantial fraction of the stellar disc.

Further care is warranted in interpreting observational biases in polarization fraction, particularly at metre-wavelengths where growth-rates for the harmonic are very high. Fundamental plasma emission and cyclotron emission are 100 per cent polarized, al-

though the observed fraction may be smaller due to geometric and propagation effects. Second harmonic emission, on the other hand, requires somewhat contrived circumstances to achieve high polarization fractions: the cyclotron frequency should be high enough but not too high to prevent the escape of radiation. Hence if a survey selects for a high polarization fraction, it is conceivable that second harmonic bursts with high polarization fractions are detected, albeit in a narrow frequency range. However, in a polarization-fraction blind survey, a prototypical second harmonic burst is unlikely to be highly polarized.

2.3 Bandwidth and duration

Both plasma and cyclotron emission are inherently narrow-band ($\Delta\nu/\nu \lesssim 0.01$) but coronae and magnetosphere are known to have a wide range of density and magnetic field variation. Hence emission bandwidth itself is not a clear discriminant between emission mechanisms.

Cyclotron maser has extremely high growth rates ($\sim 10^{-4}\nu_c\ \mathrm{s}^{-1}$ which can lead to wave growth from the thermal level of the plasma ($\sim 10^8$ K typically) to brightness temperatures of 10^{15} K (i.e. about 17 *e*-foldings) in just $\sim$2 ms. Observation of temporal structure on ms-time-scales almost always implies a cyclotron maser origin.

The duration of cyclotron maser emission is largely a geometric effect. The emission from a given site is beamed along the surface of a cone whose axis is parallel to the ambient magnetic field, which has a large opening angle and small thickness, although propagation effects can alter this simple geometry. In addition, depending on the mechanism of electron acceleration, the emitting electron may be restricted to a small azimuthal sector. This is the case when the emission is powered via electrodynamic interaction with an orbiting satellite. On the other hand, if the emission is powered by the breakdown of co-rotation between the plasma and the co-rotating magnetic field, then the emitting electron occupy all azimuthal angles. As such, depending on the rotation period of the star and the orbital period of planets that may be inducing the emission, the duration of over which the emission cone points to an observer can vary widely from minutes to several hours or even days.

Langmuir waves leading to plasma emission can grow over millisecond time-scales (see for e.g. equation 7 of Zaĭtsev & Stepanov 1983), but the rate of conversion of Langmuir waves to transverse electromagnetic waves sets the bottleneck in extracting short-duration bursts via the plasma mechanism. For instance, the growth rates of emission at metre-wavelengths (see equations B2 and B3) is $\sim 10\ \mathrm{K\,cm}^{-1}$. Hence assuming a group-velocity comparable to *c*, high brightness temperatures can build over a second. This sets the characteristics rise-time of fundamental plasma emission, which agrees with the time-scales observed in impulsive Type-III bursts (Reid & Ratcliffe 2014). There is no strict upper limit to the duration of plasma emission. So long as turbulent energy is injected into the corona, the emission will persist.

The treatment of plasma emission presented here (especially the brightness temperatures calculated in Section 2.2), assumes a Langmuir wave turbulence that is isotropic and has a flat spectrum. At the point of injection of hot plasma, the Langmuir waves are confined to a narrow forward cone. A flat spectrum is thought to develop first via spontaneous scattering of Langmuir waves packets along wavenumber space by thermal ions, and later, via induced scattering. Spontaneous scattering of Langmuir waves into other Langmuir waves by thermal ions proceeds on a time-scale, τ_L, of (equation 3.12 of Kaplan & Tsytovich 1973, where $\tau_\mathrm{L} \sim W_\mathrm{k}/J_\mathrm{k}$ in their notation)

$$\tau_\mathrm{L} \sim \nu_{100}^{-2} T_6^{1.5}\ \mathrm{min}. \tag{10}$$

The time-scale for induced scattering is evaluated in the Appendix D and for a peak turbulence value of $w \sim 10^{-5}$ is somewhat smaller. Hence, I take equation (10) to describe the time-scale over which a flat and isotropic Langmuir wave spectrum forms.

On a time-scale shorter than τ_L, if the incident turbulent energy is concentrated into a narrow cone of opening angle Ω_L and wavenumber range $\Delta k^{'}$, then the spectral energy density of Langmuir waves (and hence their temperature) compared to the isotropic case for the same overall energy density is larger by the factor $4\pi\Omega_L^{-2}(k_\mathrm{max} - k_\mathrm{min})/\Delta k'$. Hence, on time-scales comparable to of less than τ_L the bounds on brightness temperature computed in Section 2.2 can be readily exceeded by this large factor (Melrose 1980; Vedantham 2020). Therefore, at metre-wavelengths, I make a distinction between short bursts (on minute time-scales or less) and long bursts (on tens of minutes time-scales and longer). The brightness temperature limits of Section 2.2 only strictly apply to the latter.

3 DISCUSSION

3.1 Application to metre-wave detections

I now apply the theory developed in Section 2 to metre-wave observations. Details of the observations are given in Table 1. Long-duration polarized bursts from AD Leo were reported at $\sim$300 MHz by Villadsen & Hallinan (2019), whereas Lynch et al. (2017a) reported bursts from UV Ceti at 150 MHz. Both of these are highly active flare stars. As a contrast, I also consider the long-duration polarized emission from the quiescent star, GJ 1151, reported by Vedantham et al. (2020). As a reference value, the table lists the 'observed' brightness temperature assuming that the source is a filled disc with a radius given by the stellar radius. I have used the empirical scaling laws of Johnstone & Güdel (2015) to convert the observed X-ray luminosity of the stars (upper limit in case of GJ 1151) to the temperature of the thermal plasma.

In Figs 2–4, I have plotted the maximum brightness temperature feasible from fundamental and second harmonic plasma emission for the three stars as a function of the emission frequency and the temperature of the impulsively heated hot plasma component. The curves are computed using equations presented by Stepanov et al. (2001) and share a characteristic profile. The declining efficient of harmonic emission at higher frequencies and the increased collisional damping rate at higher frequencies lead to a monotonically decreasing curve for the harmonic component. The fundamental component rises quasi-linearly at low frequencies due to spontaneous emission as approximated by the relationships in Section 2. At frequencies around 1 GHz, it grows non-linearly due to induced emission, and eventually declines at higher frequencies as the collisional damping rate overcomes the rate of induced emission. I note here that the equations of Stepanov et al. (2001) for the fundamental component only consider the conversion of Langmuir to electromagnetic waves. They do not include the inverse process. In particular, the induced conversion of electromagnetic waves to Langmuir waves will ultimately limit the temperature of the electromagnetic waves. A detailed discussion of the highest brightness temperature possible for fundamental plasma emission is unnecessary for our purposes here. Suffice it to say that the brightness temperatures we are dealing with here are well within the limiting value (see e.g. Stepanov et al. 2001).

Table 1. Relevant properties of the corona and radio emission of the stars considered here. The data sources are as follows. S1: Mann et al. (2015); S2: Gaia Collaboration (2018); S3: Villadsen & Hallinan (2019); S4: Kirkpatrick, Henry & McCarthy (1991); S5: Geyer, Harrington & Worley (1988); S6: Audard, Güdel & Skinner (2003); S7: Lynch et al. (2017a); S8: Wright et al. (2018); S9: Vedantham et al. (2020).

Parameter	AD Leo	UV Ceti	GJ 1151	Data source
Sp. type	M3.4	M6	M4.5	(S1,S4,S1)
Distance (pc)	4.97	2.69	8.04	(S2,S2,S2)
Mass ($M_\odot$)	0.406	0.1	0.154	(S1,S5,S1)
Radius ($R_\odot$)	0.435	0.15	0.19	(S1,S5,S1)
L_X (ergs s^{-1})	$10^{28.92}$	$10^{27.1}$	$<10^{26.2}$	(S3,S6,S8)
F_X (ergs s^{-1} cm^{-2})	$10^{5.75}$	$10^{5.86}$	$<10^{4.88}$	$= L_X/(4\pi R_*^2)$
$T_{\rm cor}$ (10^6 K)	3.5	3.7	<2	$= 0.11 F_X^{0.26}$
$h_{\rm p}$	$0.324R_*$	$0.48R_*$	$<0.2R_*$	
$\log_{10} T_{\rm b}$ (observed[a])	12.8, 12.1	12.5, 13.3	12.3	(S3,S7,S9)
Pol. frac	> 96%, > 87%	> 27%	$64 \pm 6\%$	(S3,S7,S9)
Polarity (LCP/RCP)	Unknown	Both	RCP	(S3,S7,S9)
Duration	$>3.5^{\rm h}$	$0.5^{\rm h}$	$>8^{\rm h}$	(S3,S7,S9)
$\log_{10} L_R$ [ergs/s/Hz]	14.28	14.91	13.8	(S3,S7,S9)
Visible pole	S	N	Unknown	(S3,S7,S9)

[a]Observed $T_{\rm b}$ is computed with a projected source size $= \pi R_*^2$.

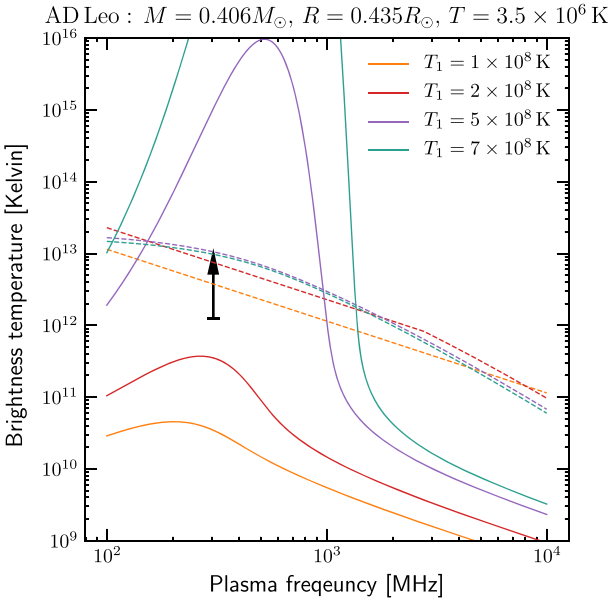

Figure 2. Peak radiation brightness temperature of fundamental (solid lines) and second harmonic (dashed lines) plasma emission for parameters relevant to AD Leo. The different curves are for different temperatures of the hot plasma component. The black arrow square shows the observationally inferred lower limit computed by assuming that the transverse size of the emitter is the same as that of the stellar disk. The black bar at the base of the arrow spans the observed bandwidth of emission. The quasi-linear rise of the fundamental curve low-frequencies is consistent with equation (6). The approximately flat profile of the second-harmonic curve at low frequencies is consistent with equation (7).

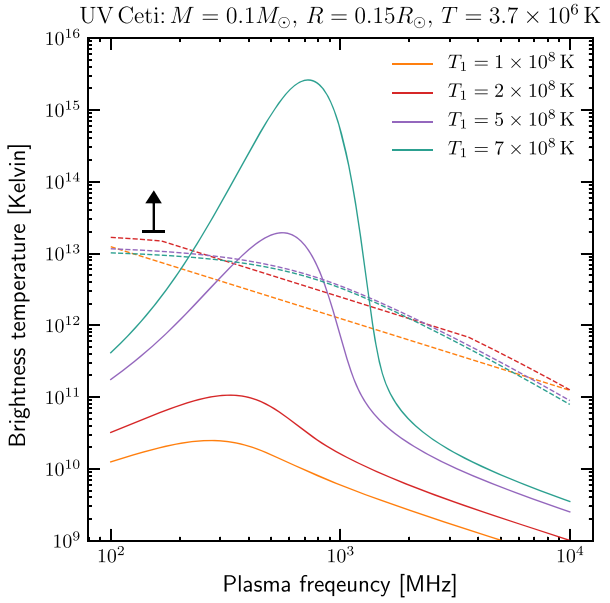

Figure 3. Same as Fig. 2 but for parameters relevant to UV Ceti. Fundamental plasma emission can only account for the observed radio emission if the entire stellar disk has active coronal loops with a saturated level of turbulence.

3.1.1 AD Leo

Villadsen & Hallinan (2019) reported two bursts from the flare star AD Leo between 290 and 320 MHz which flux densities of 38 and 210 mJy. The brighter of the two bursts only lasted about 5 min and I classify this as a short-duration burst vis-a-vis plasma emission (see Section 2.3). The second, weaker burst which is listed in table 1 lasted more than $3.5^{\rm h}$ and is a long-duration event. Although weaker, the latter provides a cleaner constraint on plasma emission models because an isotropic spectrum of turbulence can be assumed while computing the spectral density of Langmuir waves.

For the long-duration event, the high polarization fraction rules out second harmonic emission, which leaves us with fundamental plasma emission and cyclotron emission. From Fig. 2, it is evident that a hot component temperature of $T_1 \sim 10^{8.6}$ K, can account for the observed emission even if only a fraction of the stellar disc is filled with flaring coronal loops emitting fundamental plasma emission. The observed brightness temperature can be trivially supported by a loss-cone cyclotron maser (see equation 4). Therefore, for this star, the emission mechanism for the observed 300 MHz emission

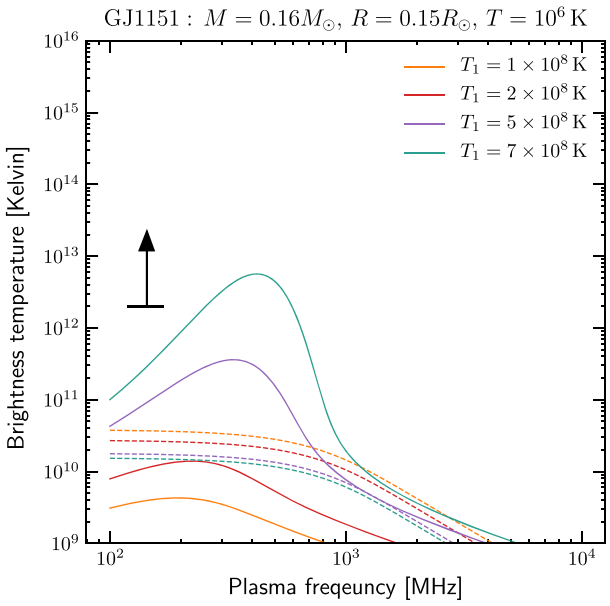

Figure 4. Same as Fig. 4 but for parameters relevant to GJ 1151. The low coronal density scale height, as implied by X-ray luminosity limits, makes the fundamental plasma emission hypothesis untenable.

cannot be readily identified based on the brightness temperature and polarized fraction.

3.1.2 UV Ceti

Lynch et al. (2017a) detected bursts from UV Ceti only in polarized emission providing a lower limit on the polarized fraction of about 27 per cent which is insufficient to rule out second harmonic plasma emission. Hence both fundamental and harmonic plasma emission, as well as cyclotron-maser emission must all be considered. Fig. 3 shows that fundamental plasma emission is untenable. Second harmonic plasma emission is feasible only if the entire stellar disc is filled by hot plasma with temperature $T_1 \gtrsim 7 \times 10^8$ K at the theoretical maximum level of turbulence. This is unprecedented as it requires the entire surface of the star to flare simultaneously instead of a few active coronal loops as seen on the Sun. I therefore conclude that the emission from UV Ceti is driven by cyclotron maser.

3.1.3 GJ 1151

Vedantham et al. (2020) present long-duration polarized emission from the quiescent star GJ 1151 at 150 MHz. GJ 1151 provides an immediate contrast because it is a quiescent star with a low (thus far undetected) X-ray emission. The observed polarization fraction rules out second harmonic plasma emission. Fig. 4 shows that even in a contrived case where the entire surface of the star is filled with simultaneously flaring coronal loops, plasma emission cannot supply the observed brightness temperature. The low frequency of observation and the high observed brightness temperature, therefore, lead to a cyclotron maser interpretation for GJ 1151.

The large impact of GJ1151's quiescence on the peak plasma brightness temperature estimates is noteworthy. This is apparent if one compares the curves in Fig. 4 and those in Figs 2 and 3. The reason for this disparity is the low coronal temperature of GJ1151 (determined from its X-ray faintness). A low coronal temperature leads to lower emissivity at the harmonic (see equation 7), and a lower density scale height over which the emission at either the fundamental of the harmonic can grow. The disparate scale height leads to large disparities in fundamental emission at higher frequencies ($\nu \sim 1$ GHz) where induced emission (maser effect) becomes dominant.

3.1.4 EQ Peg

Villadsen & Hallinan (2019) report a 0.27 Jy burst from EQ Peg at 350 MHz which is > 70 per cent circularly polarized. EQ Peg has stellar parameters similar to the UV Ceti system, using which, we get $T_b \approx 10^{14}$ K. The similarity with UV Ceti also implies that Fig. 3 is applicable to UV Ceti which clearly shows that plasma emission cannot account for the observed brightness temperature. The emission from EQ Peg observed by Villadsen & Hallinan (2019) is therefore due to cyclotron maser emission.

3.2 Comparison to cm-wave detections

Villadsen & Hallinan (2019) also report higher frequency long-duration emission from AD Leo and UV Ceti. The brightest of these reach 64 mJy between 1 and 1.6 GHz on AD Leo, and 30 mJy between 1 and 6 GHz on UV Ceti. The peak brightness temperatures of the bursts on the two stars are $T_b \approx 10^{11.2}$ K. Figs 2 and 3 show that this brightness temperature can be readily achieved with fundamental plasma emission even if an isolated active region on the star is responsible for the radio emission. The intensity of emission and the polarization fraction alone cannot be used to distinguish between the two plausible mechanisms.

3.3 Conclusions and outlook

New stellar radio observations have identified long-duration metre-wave bursts of coherent emission. Coherent plasma emission and cyclotron maser directly probe the ambient electron density and magnetic field. As such the metre-wave data can provide an understanding of the component of dMe coronae that is much more tenuous that the component probed by cm-wave observations and X-ray data.

I have endeavoured to identify the origin of metre-wave emission observed from observations of the flare stars AD Leo and UV Ceti and the quiescent star GJ 1151. My overarching conclusion is that unlike the cm-wave regime, at sufficiently low frequencies ($\nu \sim 10^2$ MHz), brightness temperatures exceeding $\sim 10^{12}$ K over hour-long duration are unlikely to be generated by fundamental plasma emission for the vast majority of M-dwarf coronal parameters. This allows us to identify the emission mechanism— the first and necessary step in determining coronal parameters.

While this paper has brought the polarized fraction, brightness temperature, and temporal duration of emission to bear, the sense of polarization (x- or o-mode) has not been considered as an identifier of the emission mechanism. This will require a treatment of the beaming properties of plasma and cyclotron maser emission as well as wave propagation effects within coronae; I leave this for future work.

ACKNOWLEDGEMENTS

I thank Prof. Gregg Hallinan and Prof. Robert Bingham for discussions, Dr Joe Callingham for commenting on an earlier version of the manuscript, and the anonymous referee for catching a crucial mistake in my brightness temperature calculations.

DATA AVAILABILITY

The code used to generate the plots in this paper is available from the author upon reasonable request.

REFERENCES

Audard M., Güdel M., Skinner S. L., 2003, ApJ, 589, 983
Bastian T. S., Dulk G. A., Leblanc Y., 2000, ApJ, 545, 1058
Benz A. O., 1993, Astrophysics and Space Science Library, Vol. 184, Kluwer, Dordrecht
Ergun R. E., Carlson C. W., McFadden J. P., Delory G. T., Strangeway R. J., Pritchett P. L., 2000, ApJ, 538, 456
Gaia Collaboration, 2018, A&A, 616, A1
Geyer D. W., Harrington R. S., Worley C. E., 1988, AJ, 95, 1841
Gupta Y. et al., 2017, Curr. Sci., 113, 707
Johnstone C. P., Güdel M., 2015, A&A, 578, A129
Kaplan S. A., Tsytovich V. N., 1973, International Series of Monographs in Natural Philosophy. Pergamon Press, Oxford
Kirkpatrick J. D., Henry T. J., McCarthy D. W., 1991, ApJS, 77, 417
Lynch C. R., Lenc E., Kaplan D. L., Murphy T., Anderson G. E., 2017a, ApJ, 836, L30
Lynch C. R., Murphy T., Kaplan D. L., Ireland M., Bell M. E., 2017b, MNRAS, 467, 3447
Mann A. W., Feiden G. A., Gaidos E., Boyajian T., von Braun K., 2015, ApJ, 804, 64
Melrose D. B., 1980, Space Sci. Rev., 26, 3
Melrose D. B., Dulk G. A., 1982, ApJ, 259, 844
Melrose D. B., Dulk G. A., Smerd S. F., 1978, A&A, 66, 315
Melrose D. B., Dulk G. A., Gary D. E., 1980, Proc. Astron. Soc. Aust., 4, 50
Murphy T. et al., 2015, MNRAS, 446, 2560
O'Gorman E., Coughlan C. P., Vlemmings W., Varenius E., Sirothia S., Ray T. P., Olofsson H., 2018, A&A, 612, A52
Reid H. A. S., Ratcliffe H., 2014, Res. Astron. Astrophys., 14, 773
Slee O. B., Willes A. J., Robinson R. D., 2003, PASA, 20, 257
Speirs D. C., Bingham R., Cairns R. A., Vorgul I., Kellett B. J., Phelps A. D. R., Ronald K., 2014, Phys. Rev. Lett., 113, 155002
Stepanov A. V., Fuerst E., Krueger A., Hildebrandt J., Barwig H., Schmitt J., 1995, A&A, 299, 739
Stepanov A. V., Kliem B., Krüger A., Hildebrandt J., Garaimov V. I., 1999, ApJ, 524, 961
Stepanov A. V., Kliem B., Zaitsev V. V., Fürst E., Jessner A., Krüger A., Hildebrandt J., Schmitt J. H. M. M., 2001, A&A, 374, 1072
Tingay S. J. et al., 2013, PASA, 30, e007
Treumann R. A., 2006, A&AR, 13, 229
Turner J. D., Grießmeier J.-M., Zarka P., Vasylieva I., 2019, A&A, 624, A40
van Haarlem M. P. et al., 2013, A&A, 556, A2
Vedantham H. K., 2020, A&A, 639, L7
Vedantham H. K. et al., 2020, Nat. Astron., 4, 577
Villadsen J., Hallinan G., 2019, ApJ, 871, 214
Wright N. J., Newton E. R., Williams P. K. G., Drake J. J., Yadav R. K., 2018, MNRAS, 479, 2351
Wu C. S., Lee L. C., 1979, ApJ, 230, 621
Zaitsev V. V., Stepanov A. V., 1983, Sol. Phys., 88, 297
Zaĭtsev V. V., Shaposhnikov V. E., Rucker H. O., 2005, Astron. Rep., 49, 327
Zic A. et al., 2019, MNRAS, 488, 559
Zlotnik E. I., 1981, A&A, 101, 250

APPENDIX A: GYRO-HARMONIC OPTICAL DEPTH

Although cyclotron maser emission is emitted by mildly relativistic electrons, the thermal background electrons can resonantly absorb the emitted waves at harmonics of the cyclotron frequency. The emitted radiation must necessarily pass through layers with decreasing field strength where absorption at the higher harmonics of the cyclotron frequency (gyro-harmonic absorption hereafter) can be catastrophic for radiation escape. The optical depth for the o- and x-mode are given by (Stepanov et al. 1995)

$$\tau_{\rm o,x} = \pi \left(\frac{\omega_{\rm p}}{\omega_{\rm c}}\right)^2 \frac{\omega L_{\rm B}}{c} \frac{s^{2s-2}}{s!} \left(\frac{2k_{\rm B}T\sin\theta}{m_{\rm e}c^2}\right)^{2s-2} C_{\rm o,x}, \tag{A1}$$

where $s \geq 2$ is the harmonic at which the optical depth is being computed, $L_{\rm B} = B|\Delta B|^{-1}$ is the magnetic scale length, $m_{\rm e}$ is the electron mass, T is the plasma temperature, and $C_{\rm o,x}$ is a mode dependent factor:

$$C_{\rm o,x} = \mu_{\rm o,x}^{2s-3} \frac{(1 + T_{\rm o,x}\cos\theta + K_{\rm o,x}\sin\theta)^2}{1 + T_{\rm o,x}^2}. \tag{A2}$$

Here $\mu_{\rm o,x}$ is the refractive index, $T_{\rm o,x}$ and $K_{\rm o,x}$ are the transverse and longitudinal axial ratios. They are given by

$$\begin{aligned} T_{\rm o} = -T_{\rm x}^{-1} &= \frac{Y(1-X)\cos\theta}{0.5Y^2\sin^2\theta - \Delta} \\ \Delta &= 0.25Y^4\sin^4\theta + (1-X)^2Y^2\cos^2\theta \\ K_{\rm o,x} &= \frac{XY\sin\theta}{1-X}\frac{T_{\rm o,x}}{T_{\rm o,x} - Y\cos\theta} \\ \mu_{\rm o,x}^2 &= 1 - \frac{XT_{\rm o,x}}{T_{\rm o,x} - Y\cos\theta}, \end{aligned} \tag{A3}$$

where $X = \nu_{\rm p}^2/\nu^2$, $Y = \nu_{\rm c}/\nu$. We will use the above expression for $C_{\rm o,x}$ in our computations, but for a quick estimate one can use $C_{\rm o,x} \approx \sqrt{\pi/2}[0.5(1 - \sigma|\cos\theta|)]^2$ where $\sigma = 1$ for the o-mode and $\sigma = -1$ for the x-mode. Fig. A1 shows the gyro-harmonic optical depth at 150 MHz as a function of the angle between the wave-vector and the magnetic field, θ, and plasma to cyclotron frequency ratio, $\nu_{\rm p}/\nu_{\rm c}$. The optical depths have been computed for propagation over $L = 10^{10}$ cm which is comparable to the density scale heights of stellar coronae. Because the radiation is emitted at $\theta \sim \pi/2$, emission at the fundamental is near completely absorbed in the $s = 2$ layer unless $\nu_{\rm p}/\nu_{\rm c} \lesssim 10^{-3}$ which for emission at 150 MHz corresponds to an ambient thermal plasma density of just $\sim$300 cm^{-3}. Emission at the second harmonic will suffer catastrophic absorption at the third harmonic layer unless $\nu_{\rm p}/\nu_{\rm c} \lesssim 10^{-2}$ which for emission at 150 MHz corresponds to a thermal plasma density of $\approx$7000 cm^{-3}. For comparison, typical base pressure in the solar corona range between 10^8 and 10^9 cm^{-3}. The energy density in a cyclotron maser at metre-wavelengths can be extremely high ($T_{\rm b} \gtrsim 10^{14}$ K). This allows escape of radiation at $\gtrsim 10^{12}$ K brightness temperature despite moderate levels of gyro-harmonic optical depth. As such a conservative limit for significant radiation to escape would be $\nu_{\rm p}/\nu_{\rm c} < 0.01$. Incidentally, $\nu_{\rm p}/\nu_{\rm c} < 0.01$ also corresponds to the absolute limit of $(\nu_{\rm p}/\nu_{\rm c})^2 < 0.5(1 - \gamma^{-1})$ at which a shell-type maser with $\beta = 0.2$ electrons is theoretically feasible (equation 1 of Ergun et al. 2000).

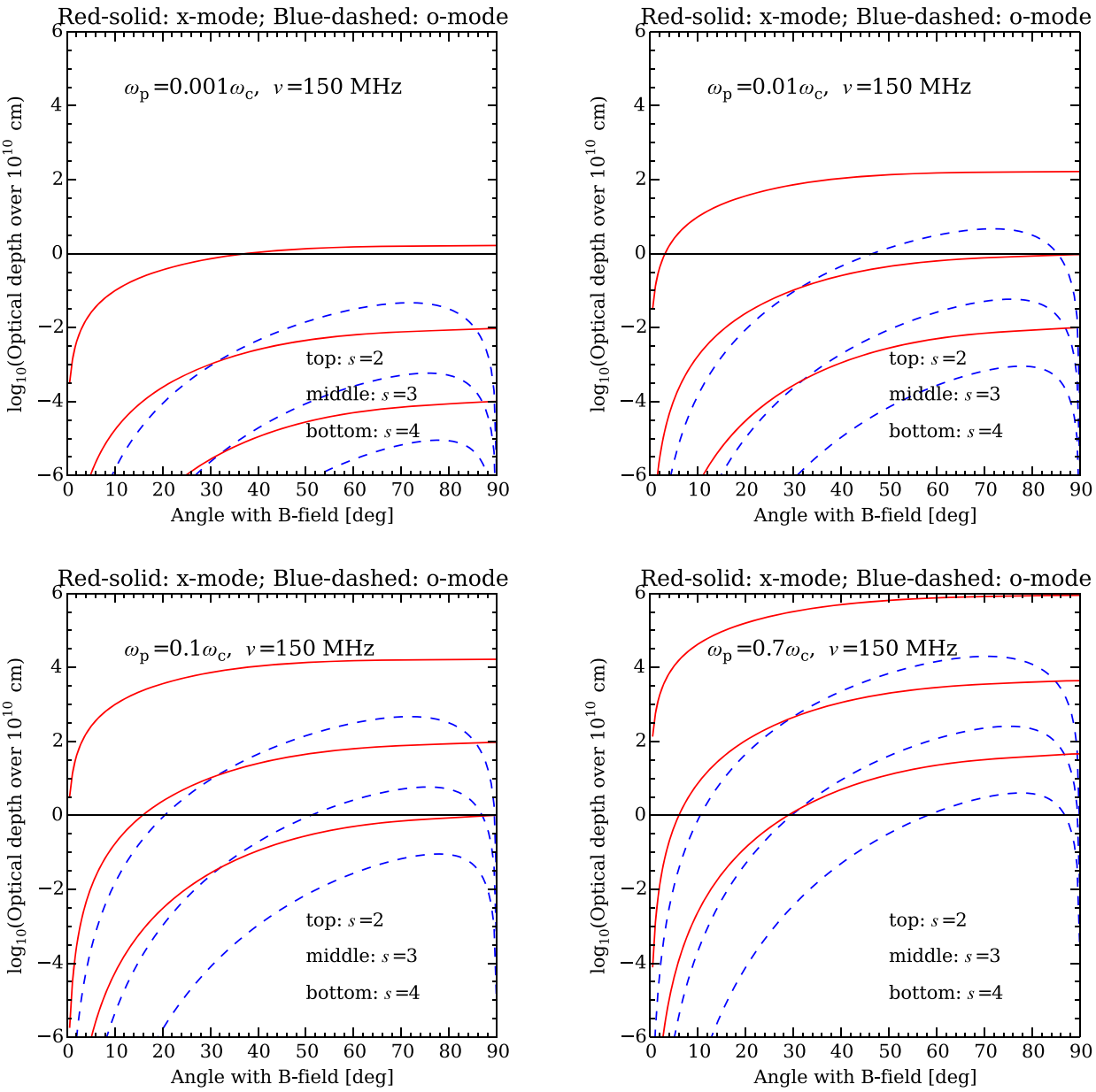

Figure A1. Gyro-harmonic optical depth at different harmonics of the cyclotron frequency for the x- and o-mode radiation as a function of the angle between the wave-vector and the ambient magnetic field. Each panel assumes a different plasma to cyclotron frequency ratio. All panels assume radiation at $\nu = 150$ MHz and a scale length of $L = 10^{10}$ cm. The optical depth scales as $\tau \propto L\nu(\nu_p/\nu_c)^2$.

Table A1. Glossary of symbols and their meaning.

R_*	Stellar radius
$R_{*,10}$	$R_*/(10^{10}$ cm)
d	Distance to the star
d_{10}	$d/(10$ pc)
B	Magnetic field strength
n_0	Hot plasma density
ν	Spectral frequency
ν_{100}	$\nu/(100$ MHz)
ω	Angular frequency $= 2\pi\nu$
λ	Wavelength
k	Electromagnetic wave-vector $= 2\pi/\lambda$

Table A1 – *continued*

R_*	Stellar radius
k'	Langmuir wave-vector $= 2\pi/\lambda$
ν	Electromagnetic wave frequency
$\Delta\nu$	Emission bandwidth
ν_p	Plasma frequency
ν_c	Cyclotron frequency
ν_{uh}	Upper hybrid frequency
ω_p	Angular plasma frequency ($=2\pi\nu_p$)
ω_c	Angular cyclotron frequency ($=2\pi\nu_c$)
ω_{uh}	Angular upper hybrid frequency ($=2\pi\nu_{uh}$)
θ	Angle between electromagnetic wave vector and magnetic field

Table A1 – *continued*

R_*	Stellar radius
θ'	Angle between Langmuir wave vector and magnetic field
h_p	Density scale height
k_B	Boltzmann's constant
c	Speed of light
v_e	Electron thermal velocity
v_0	Hot plasma electron speed (cyclotron emission)
v_1	Hot plasma electron thermal speed (plasma emission)
β	velocity in units of c
$\beta_{0.2}$	$\beta/0.2$
Γ	Maser growth rate
L	Length scale of the magnetic trap
m_e	Electron mass
W_L^{tot}	Langmuir wave energy density
w	Fractional kinetic energy in turbulence
F	Flux density
f	Fraction of stellar disc filled with flaring loops
s	Cyclotron harmonic number
T	Plasma temperature
T_1	Hot plasma component temperature
T_b^L	Langmuir wave's brightness temperature
$T_{b,h}$	Brightness temperature of harmonic plasma emission
$T_{b,f}$	Brightness temperature of fundamental plasma emission
T_b^{obs}	Observed brightness temperature
T_b^{max}	Peak brightness temperature of cyclotron maser emission
T_b^{avg}	Average brightness temperature of cyclotron maser emission
τ_L	Time-scale for angular scattering of Langmuir waves
$W_{k'}$	Spectral energy density of Langmuir waves
Ω_L	Beam solid angle of Langmuir waves
o, x	Ordinary and extraordinary magnetoionic modes
$\tau_{o,x}$	Cyclotron optical depth
L_B	Magnetic scale length
$\mu_{o,x}$	Magnetoionic refractive index
$T_{o,x}$	Transverse magnetoionic axial ratio
$K_{o,x}$	Longitudinal magnetoionic axial ratio
λ_D	Plasma Debye length $=v_e/\omega_p$
r_0	Classical electron radius
L_X	Soft X-ray luminosity ($\sim$0.1 to $\sim$10 keV)
$\alpha_{f,h}$	Fundamental and second harmonic emissivity for plasma emission

APPENDIX B: LOW-FREQUENCY APPROXIMATION FOR THE BRIGHTNESS OF PLASMA EMISSION

Non-thermal growth of Langmuir waves is feasible with kinetic instabilities such as a bump-on-tail or loss-cone instability that typically yield a flat spectrum ($W_{k'}$ independent of k'; Kaplan & Tsytovich 1973) over a range of wavenumbers: $k' \in [k'_{min}, k'_{max}]$. In case of a loss-cone instability that likely operates in flaring loops, $k'_{min} = \omega_p/v_1$ and $k'_{max} = \omega_p/(3v_e)$ (Zaĭtsev & Stepanov 1983). The former is obtained from the condition for resonance that requires the phase velocity of Langmuir waves to be equal to the velocity of hot electrons. The latter is a necessary to ensure that Landau damping by thermal electrons does not arrest wave growth.

The bandwidth of emission can be derived from the dispersion relationship for Langmuir waves: $\omega_L^2 = \omega_p^2(1 + 3k'^2\lambda_D^2)$, where $\lambda_D = v_e/\omega_p$ is the Debye length. The resulting bandwidth is

$$\frac{\Delta\nu}{\nu} \approx \left(1 + 3k'^2_{max}\lambda_D^2\right)^{1/2} - \left(1 + 3k'^2_{min}\lambda_D^2\right)^{1/2} \approx \frac{3}{2}\lambda_D^2\left(k'^2_{max} - k'^2_{min}\right). \quad \text{(B1)}$$

The emissivity for the fundamental and harmonic are given by

$$\alpha_f = \frac{\pi}{36}\frac{m_e v_1^2}{k_B}\frac{w\omega_p^2}{\sqrt{3}k' v_e c} \quad \text{(B2)}$$

and

$$\alpha_h = \frac{(2\pi)^5}{15\sqrt{3}}\frac{c^3}{\omega_p^2 v_1}\frac{w^2 n_e T}{\xi^2} \quad \text{(B3)}$$

where the fractional power in turbulence $w = W_L^{tot}/(nk_BT)$ (W_{tot}^L is the energy density of Langmuir waves) and the spectral bandwidth $\xi = (4\pi/3)\lambda_D^3(k^3_{max} - k^3_{min})$. Note that the units of α_f and α_h above are Kelvins of brightness temperature per unit length. To get the brightness temperature we must multiply this emissivity with the length-scale over which the ambient plasma frequency does not vary by more than the instantaneous bandwidth of emission. Hence $T_{b,f} = 2\alpha_{f,h}h_p\Delta\nu/\nu$ which yield equations (6) and (7).

Finally, the brightness temperature of an isotropic distribution of Langmuir waves is given by $T_b^L k_B = (2\pi)^3 W_{k'}/k'^2$, where $\int dk' W_{k'}$ is the volume energy density of Langmuir waves per unit solid angle. For an isotropic flat spectrum of Langmuir-wave turbulence $W_{k'}$ is independent of k' and we have $4\pi W_{k'}(k'_{max} - k'_{min}) = W_L^{tot} = w \times (nk_BT)$. To get a conservative order of magnitude upper bound on the brightness of Langmuir waves, we set $w = 10^{-5}$, $k' \approx k'_{min} = \omega_p/v_1$, $k'_{max} - k'_{min} \approx k'_{max} = \omega_p/(3v_e)$ to get

$$T_b^L \lesssim \frac{3}{4\pi}\frac{nTwv_e v_1^2}{v_p^3} \quad \text{(B4)}$$

which gives equation (8).

APPENDIX C: POLARIZATION OF SECOND HARMONIC PLASMA EMISSION

Theoretical investigation into the polarization of transverse emission at the second harmonic due to coalescence of two Langmuir waves can be found in Melrose, Dulk & Smerd (1978), Zlotnik (1981), and Melrose et al. (1980). Here we make use of the formulae given by Melrose et al. (1980, their equations 1–4). The degree of isotropy of the Langmuir wave spectrum enters the equations through the factors A, B, and C in their equations (2a) through to (2c). For the purely isotropic case, we have $<\cos^0\theta'> = 2$, $<\cos^2\theta'> = 2/3$ and $<\cos^4\theta'> = 2/5$, which gives $A \approx 0.133$, $B = 0$ and $C = 0$.

Higher polarization fractions are obtained for higher values of ν_c/ν_p. However some care is needed in interpreting emission and propagation issues where the ratio is of order unity. This is due to two factors: (a) Gyro-harmonic absorption may preclude detectable radiation from escaping the source for $\nu_c \sim \nu_p$. Additionally, the Langmuir waves are actually excited not just above the plasma frequency but rather the upper hybrid frequency given by $\omega_{uh} \approx \sqrt{\omega_p^2 + \omega_c^2\sin^2\theta}$. (b) A large magnetic field may prevent Langmuir waves from achieving isotropy thereby modifying the polarization properties of the emission.

From Fig. A1, it is clear that for ν_c/ν_p much larger than 0.1, even the $s = 4$ layer can have prohibitive levels of absorption. We therefore enforce the condition $2\nu_{uh} > 4\nu_c$ (factor of 2 is for second harmonic emission) to avoid catastrophic gyro-harmonic absorption, which gives $\nu_c/\nu_p < (4 - \sin^2\theta)^{-1/2}$. The right-hand side varies between 0.5 and 0.577 as θ increases from 0 to $\pi/2$. We note that due to the low x-mode gyro-harmonic absorption at $\theta \approx 0$, somewhat higher values of ν_c/ν_p may lead still lead to escaping radiation but this would require a contrived geometry. While this is certainly feasible in some

cases where the star is viewed pole-on, but it cannot be true of the vast majority of observed events.

The non-isotropic spectrum of Langmuir waves in the presence of a magnetic field has been discussed by Melrose et al. (1978). The growing wave-spectrum is confined to forward and backward cones of opening angle $\theta' \lesssim \sin^{-1}(\sqrt{3}k'v_e/\omega_c)$. Letting the Langmuir wavenumber $k' = k_{max} = \omega_p/(3v_e)$, we get $\theta' \lesssim \sin^{-1}[\nu_p/(\sqrt{3}\nu_c)]$. Within the gyro-harmonic constraint of $\nu_c/\nu_p \lesssim 0.577$, the argument of $\sin^{-1}$ is larger than unity, implying that the field does not restrict waves from growing isotropically. For $\nu_c/\nu_p \gtrsim 0.6$ however, wave growth is restricted, but escape from gyro-harmonic absorption is only possible at low θ. We have denoted by using dotted lines in Fig. 1.

APPENDIX D: TIME-SCALE FOR LANGMUIR SPECTRAL EVOLUTION BY INDUCED SCATTERING

The growth rate of Langmuir waves due to induced scattering on thermal ions is approximately given by (Kaplan & Tsytovich 1973, their equations 3.17 & 3.18) $\Gamma_L \approx \alpha \partial W_{k'}/\partial k'$, where $\alpha = \pi\omega_p^3/(108nm_p v_e^4)$. The time-scale over which induced scattering affects the spectrum substantially is therefore given by $\tau_L = \Gamma_L^{-1}$. To evaluate τ_L in an order-of-magnitude sense, we can set $\partial W_{k'}/\partial k' \sim W_{k'}/k_{min} = wnk_B T/(4\pi k_{min}k_{max})$ where we have assumed that $W_{k'}$ is quasi-linear as the final flat Langmuir wave spectrum is forming. Using $k_{max} = \omega_p/(3v_e)$, the Landau damping scale and $k_{min} = \omega_p(k_B T_1/m_e)^{-1/2}$, the resonance wavenumber, the time-scale becomes

$$\tau_L \sim \frac{144}{w\omega_p}\frac{m_p}{m_e}\left(\frac{T}{T_1}\right)^{1/2} \tag{D1}$$

Assuming a hydrogen plasma, and letting $T_1 = 30T$ as an estimate, we get the time-scale for induced scattering to be $\tau_L \sim 0.13\nu_{100}^{-1}(w/10^{-5})^{-1}$ min.

This paper has been typeset from a TEX/LATEX file prepared by the author.